GEOPHYSICS, VOL. 75, NO. 6 (NOVEMBER-DECEMBER 2010); P. E235–E246, 6 FIGS., 2 TABLES.
10.1190/1.3506561

Permeability models of porous media: Characteristic length scales, scaling constants and time-dependent electrokinetic coupling

Emilie Walker[1] and Paul W. J. Glover[1]

ABSTRACT

Fluid permeability is one of the most important characteristics of a hydrocarbon reservoir, and is described by a number of empirical and theoretical models. We have taken four of the most important models, each of which is derived from a different physical approach, and have rewritten them in a generic form that implies a characteristic scale length and scaling constant for each model. The four models have been compared theoretically and using experimental data from 22 bead packs and 188 rock cores from a sand-shale sequence in the U. K. sector of the North Sea. The Kozeny-Carman model did not perform well because it takes no account of the connectedness of the pore network and should no longer be used. The other three models (Schwartz, Sen, and Johnson [SSJ]; Katz and Thompson [KT]; and the Revil, Glover, Pezard, and Zamora [RGPZ]) all performed well when used with their respective length scales and scaling constants. Surprisingly,we found that the SSJ and KT models are extremely similar, such that their characteristic scale lengths and scaling constants are almost identical even though they are derived using extremely different approaches: The SSJ model by weighting the Kozeny-Carman model using the local electrical field, and the KT model by using entry radii from fluid imbibition measurements. The experimentally determined scaling constants for each model were found to be $c_{SSJ} \approx c_{KT} \approx 8/3 \approx c_{RGPZ}/3$. Use of these models with AC electrokinetic theory has also allowed us to show that these scaling constants are also related to the a value in the RGPZ model and the m^* value in time-dependent electrokinetic theory and then to derive a relationship between the electrokinetic transition frequency and the RGPZ scale length, which we have validated using experimental data. The practical implication of this work for permeability prediction is that the KT model should be used when fluid imbibition data are available, whereas the RGPZ model should be used when electrical data are available.

INTRODUCTION

It is arguable that the two most important characteristics of a sedimentary rock are the porosity and the permeability — that is, some measure of the maximum volume that hydrocarbons can occupy and a measure of how easily they may be extracted. The permeability of a rock (measured in m^2) is clearly defined by Darcy's law and can be qualitatively thought to depend on (1) some measure of the aperture available for fluid flow, from which the units of permeability arise, and (2) some measure of the connectedness of the flow path (Glover and Walker, 2009). The general form of the permeability equation for a porous medium therefore would be

$$k = \frac{GL^2}{c}, \tag{1}$$

where L is some length scale that, when squared, represents the aperture available for fluid flow; G is the connectedness as defined by Glover (2009) and discussed briefly in the next section; and we introduce a scaling constant c that is not the same for each model. The analysis of both the length scale and the scaling constant of each model forms the core of this paper and is discussed in detail below.

We consider four ways of defining an analytical expression for the permeability of a porous medium. The first is the well known Kozeny-Carman (KC) model, which has many forms, but the one that is of most use to us is the one used by Bernabé (1995):

$$k_{KC} = \frac{r_{KC}^2}{c_{KC}F} = \frac{Gr_{KC}^2}{c_{KC}}, \tag{2}$$

where the permeability, k_{KC}, is expressed in terms of the KC hydraulic radius, the formation factor F, a constant c_{KC}, and a length scale r_{KC}, where $r_{KC} = 2V_p/S_p$, i.e., twice the ratio of the pore volume, V_p,

Manuscript received by the Editor 9 October 2009; revised manuscript received 27 January 2010; published online 13 December 2010.
[1]Université Laval, Department of Geology and Engineering Geology, Québec, Canada. E-mail: walker.emilie@gmail.com; paglover@ggl.ulaval.ca.

to the area of the interface between the pores and the solid matrix, S_p.

The second is a model that grew from a number of papers by Schwartz, Sen, Johnson, and others, which we conventionally call the SSJ model (Johnson et al., 1986; Johnson and Sen, 1988; Schwartz et al., 1989; Johnson and Schwartz, 1989) and which is expressed as

$$k_{SSJ} = \frac{\Lambda_{SSJ}^2}{c_{SSJ}F} = \frac{G\Lambda_{SSJ}^2}{c_{SSJ}}, \tag{3}$$

where the permeability, k_{SSJ}, is expressed in terms of a length scale, Λ_{SSJ}, where $\Lambda = 2\int|\nabla\psi_o(r)|^2 dV_p / \int|\nabla\psi_o(r)|^2 dS_p$. This length scale derives from the classical hydraulic radius r_{KC} used by Kozeny and Carman. The additional terms, which amount to a dynamic averaging procedure carried out using the local electric field $\nabla\psi_o$ as a weighting factor, have the effect of reducing the effect of dead-end and other low-conducting pores (Bernabé, 1995). The constant is c_{SSJ}.

A third model is that of Katz and Thompson (1986, 1987). As pointed out by Bernabé (1995), this model is based on very different physics and relies on a capillary radius r_{KT} at breakthrough during an invasion percolation process, e.g., mercury injection, but leads to a similar equation, with the constant c_{KT}.

$$k_{KT} = \frac{r_{KT}^2}{c_{KT}F} = \frac{Gr_{KT}^2}{c_{KT}}. \tag{4}$$

A fourth model arises from Glover et al. (2006) and Glover and Walker (2009). The first of these papers used electrokinetic arguments to arrive at an equation for permeability that is based directly on equation 1. Their equation is

$$k_{RGPZ} = \frac{d^2\phi^{3m}}{4am^2}, \tag{5}$$

where RGPZ refers to the authors of a previous unpublished paper from which the work by Glover et al. (2006) evolved (Revil, Glover, Pezard, and Zamora). The permeability is expressed not in terms of a characteristic length scale of the pores but as a mean grain diameter d. The other parameters are the porosity ϕ the cementation exponent m, which is fully defined by Glover (2009); and a constant a. It is worth noting that equation 5 is the general case of the solution found for bead packs by Revil and Cathles (1999). The paper by Glover and Walker (2009) produced, again using electrokinetic arguments, a transformation between the mean grain size of a rock and an effective length scale of the pore network that has allowed equation 5 to be expressed as

$$k_{RGPZ} = \frac{r_{RGPZ}^2}{c_{RGPZ}F} = \frac{Gr_{RGPZ}^2}{c_{RGPZ}}, \tag{6}$$

which is consistent with the style of the other models. Unlike the other models, the RGPZ model requires that the constant $c_{RGPZ} = 8$.

There are many questions that need to be answered: (1) How is the tortuosity of the pore network incorporated in the general framework? (2) How are the various length scales interrelated? (3) Which values do the scaling constants c_i take? (4) Are the scaling constants simply a way of interrelating the different definitions of length scale? (5) Are then all of the models consistent with each other? Because the permeability also appears in the theory that describes the frequency-dependent electrokinetic behavior of porous media, can we find a new method of predicting permeability from AC electrokinetics? This paper is a theoretical examination of these questions.

TORTUOSITY AND CONNECTEDNESS

The preceding equations are expressed in terms of the formation factor F and the inverse formation factor G, where $G \equiv \sigma_o/\sigma_f = 1/F$, σ_o is the electrical conductivity of the rock, and σ_f is that of the fluid that saturates its pores. The value of G varies from 0, which represents the case when $\sigma_o = 0$, i.e., when $\phi = 0$, if the matrix is an insulator, and increases as the porosity increases, with $G \to 1$, i.e., $\sigma_o = \sigma_f$ as $\phi \to 1$. One can view the parameter G as a measure of the *availability* of pathways for electrical transport. That is, it is a measure of the connectedness of the pore and fracture network of a sample as defined by Glover (2009). The connectedness, G, depends on the amount of pore space available for conduction, i.e., the porosity ϕ, and the distribution of that pore volume, i.e., the connectivity, χ *via* the relationship $G = \phi\chi$. It is now possible to see that equations 1–4 and 6 all take the form

$$k = \frac{\phi\chi L^2}{c}, \tag{7}$$

where the permeability is controlled by (1) the amount of pore volume available for flow, expressed by ϕ; (2) the connectivity of that pore volume, expressed by χ; and (3) some measure of the physical aperture through which the fluid will flow, expressed by L^2. It is the last that introduces a physical scaling into the relationship.

LENGTH SCALES

The physical significance of the length scales should be understood if the models are to be compared. All of the length scales are defined in terms of physical quantities, although those parameters are not necessarily measurable on a macroscopic scale. Not all of the length scales have a well-defined physical meaning; that is they do not represent physical lengths that may be easily imagined, such as the radius of a grain.

The physical significance of the length scale r_{KC} is based on a global ratio of pore volume to the area of the interface between the pores and the solid matrix and is given by $r_{KC} = 2V_p/S_p$. If we consider a representative elementary volume of a typical porous medium of porosity ϕ and volume V, which contains spherical particles of radius r_{grain}, then the pore volume is $V_p = \phi V$ and the area of the interface between the pores and the solid matrix $S_p = 4n\pi r^2_{grain}$, where n is the number of grains; $n = 3V(1-\phi)/4\pi r^3_{grain}$. These relationships allow us to calculate the KC length scale in terms of the grain radius for spherical particles as

$$r_{KC} = \frac{2}{3}\frac{\phi}{(1-\phi)} r_{grain}, \tag{8}$$

which, interestingly, is the same for cubic particles of side length $2r_{grain}$. If a part of the porosity ϕ_c does not contribute to the fluid flow, then equation 8 may be modified to give

$$r_{KC} = A_{KC} r_{grain} = \frac{2}{3}\frac{(\phi-\phi_c)}{(1-\phi)} r_{grain}, \tag{9}$$

in the classical definition of a percolation threshold. It should be noted that Mavko and Nur (1997) introduced a percolation porosity into

the KC model and found that it gave significant improvements for clean, well-sorted rocks but at the price of having to choose the percolation porosity empirically to obtain a good fit.

Figure 1 shows how the porosity-dependent part of equation 9, which we have defined $A_{KC} \equiv 2(\phi - \phi_c)/3(1 - \phi)$, varies with porosity for $\phi_c = 0.0$, 0.1, and 0.2, respectively. Because the grain size of a monodisperse bead pack is fixed and well defined, the A_{KC} value allows us to examine how the length scale that is used in the permeability model varies with porosity. For the KC model, the A_{KC} value approaches 0 asymptotically as the porosity approaches the critical (threshold) porosity ϕ_c. This implies that as the connected porosity diminishes, the value of r_{KC} also diminishes until it is 0 and all pathways for fluid flow are sealed. The A_{KC} value remains lower than unity for values between ϕ_c and approximately 0.65, showing that, for these values, the length scale is smaller than the grain radius, which is reasonable, and becoming greater than the grain radius as the porosity increases to such an extent that the porous medium becomes a suspension of grains.

The SSJ model is a further modification to the KC model, and its length scale is given by

$$\Lambda_{SSJ} = 2\frac{\int |\nabla \psi_o(r)|^2 dV_p}{\int |\nabla \psi_o(r)|^2 dS_p}. \tag{10}$$

which represents the same V_p to S_p ratio but is weighted by the local electric field $\nabla \psi_o$. Because the local electrical field is not a macroscopically measurable quantity, the modification remains interesting but impractical. The length scale Λ_{SSJ} cannot be interpreted as a physically observable length but may be regarded as the ratio of the pore volume to the area of the interface between the pores and the solid matrix but weighted to diminish the effect of isolated and dead-end pores. Nevertheless, the results of Glover et al. (2006) showed that

$$\Lambda_{SSJ} = \frac{1}{mF} r_{grain} = \frac{1}{m\phi^{-m}} r_{grain}, \tag{11}$$

which allows the SSJ length scale also to be referred to the grain radius, where we define $A_{SSJ} = 1/mF = 1/m\phi^{-m}$ in a similar manner as we did for the KC model. Figure 1 also shows the curves for A_{SSJ} for $\phi_c = 0.0$, 0.1, and 0.2, and for $m = 1.5$, i.e., for spherical grains, whereby we have modified equation 11 to take account of a percolation threshold for the fluid flow, *viz* equation 11 becomes

$$\Lambda_{SSJ} = \frac{1}{m(\phi - \phi_c)^{-m}} r_{grain}, \tag{12}$$

and $A_{SSJ} = 1/m(\phi - \phi_c)^{-m}$. Figure 1 shows that the A_{SSJ} values are lower than those for the KC model. This is to be expected because the SSJ model preferentially ignores a certain fraction of the pore space that is not well connected and implies that the values of Λ_{SSJ} are lower than those of r_{KC} in the same sample. This is true for all values of porosity for values of $m > 1.1$ approximately, and results when the cementation exponent nears unity and the pore space is extremely well connected, so the SSJ model becomes similar to the KC model at low porosities. The SSJ model curves conform to the critical porosity threshold in the same way as the KC model and for the same reasons; however, the A_{SSJ} never becomes greater than unity, which indicates that it has some limit in its validity at high porosities.

The KT model defines its length scale pragmatically as the capillary radius r_{KT} at breakthrough during an invasion percolation process such as mercury injection. As such, the length scale is easily measurable. It may also be related to the grain size if the particles are spherical using the results of Glover and Walker (2009) together with those of Glover and Déry (2010), whence it is possible to derive

$$r_{KT} = \frac{\sqrt{3}}{R_i m F} r_{grain} = \frac{\sqrt{3}}{R_i m \phi^{-m}} r_{grain}, \tag{13}$$

where R_i is the ratio of the pore radius to the pore throat radius (capillary radius) for the degree of packing present in the porous medium. Glover and Déry (2010) have shown that $R_{cubic} = 1.767$ for cubic packing (analytically), $R_{tetr} = 1.453$ for tetragonal packing (analytically), and $R_{rand} = 1.627$ for random packing (by interpolation).

Once again, it is possible to account for a percolation threshold by rewriting equation 13 as

$$r_{KT} = \frac{\sqrt{3}}{R_i m(\phi - \phi_c)^{-m}} r_{grain}, \tag{14}$$

and $A_{KT} = \sqrt{3}/R_i m(\phi - \phi_c)^{-m}$, and once again the results of A_{KT} for $\phi_c = 0.0$, 0.1, and 0.2 and $m = 1.5$ are also shown in Figure 1. The A_{KT} values are also lower than those for the KC model (except when $m = 1$); however, the surprise is that they are extremely close to the SSJ curves. This is not an easy result to explain because the KT model is derived from very different physics to those underlying the SSJ model, and it implies that $\Lambda_{SSJ} \approx r_{KT}$; in other words, Λ_{SSJ} is a good estimator of the pore throat radius of a porous medium. The result arises because $\sqrt{3}/R_{rand} \approx 1$, where the value $\sqrt{3}$ arises from the work of Glover and Walker (2009), and the value of $R_{rand} = 1.627$ has arisen independently and solely from considerations of the geometry of grain packing in the work of Glover and Déry (2010). It is possible that the two models provide very similar results due to the manner in which fluid that flows through individual pores at a local scale pass from the viscous flow to inertial flow. This idea, which is developed in a later section, is linked to the frequency behavior of hydraulic

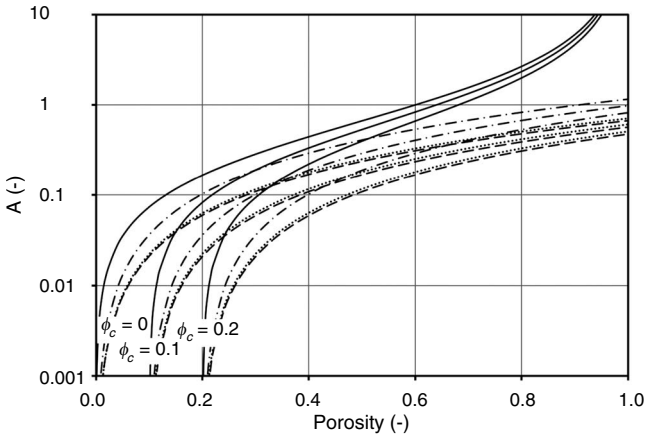

Figure 1. The value of the A coefficient as defined in this work, which links the length scale of each permeability model r_i to the common length scale provided by the radius of the grains that compose the porous medium. KC, solid lines; SSJ, long dashed lines; KT, dotted lines; RGPZ, dot-dashed lines. In each case, there is a set of three curves for values of critical porosity $\phi_c = 0.0$, 0.1, and 0.2. The KC model is independent of cementation exponent, but a cementation exponent of $m = 1.5$ is used for the other models.

flow and streaming potential and the transition frequency that is caused by the visco-inertial transition.

Finally, examining the results of the RGPZ model (Glover et al., 2006; Glover and Walker, 2009), we can see that the length scale r_{RGPZ} is defined as an effective pore size for electrical and hydraulic transport that is consistent with the electrokinetic equations from which it was derived. The derivation (Glover and Walker, 2009) provides

$$r_{RGPZ} = \frac{\sqrt{3}}{mF} r_{grain} = \frac{\sqrt{3}}{m\phi^{-m}} r_{grain}. \quad (15)$$

Once again, it is possible to account for a percolation threshold by rewriting equation 15 as

$$r_{RGPZ} = \frac{\sqrt{3}}{m(\phi - \phi_c)^{-m}} r_{grain}, \quad (16)$$

and $A_{RGPZ} = \sqrt{3}/R_i m(\phi - \phi_c)^{-m}$, and once again the results of A_{RGPZ} for $\phi_c = 0.0$, 0.1, and 0.2 and for $m = 1.5$ are also shown in Figure 1. The A_{RGPZ} values are also lower than those for the KC model (except when $m = 1$) but not as low as those for the SSJ and KT models, and, like the SSJ and KT models, there is no large increase in A_{RGPZ} as one approaches $\phi = 1$; however, the value of A_{RGPZ} can be a little larger than unity. Once again, the percolation threshold behaves in a similar manner to the other models. Overall, the RGPZ model has length scale values between those of the KC model and those of the SSJ and KT models.

In this section, we have seen that the four models have physically distinct length scales (although the SSJ and KT models are very close). Because all of the models purport to describe the same fluid permeability, the implication is that the four models should also have distinct scaling constants.

SCALING CONSTANTS

The previous sections show there to be four models that share a common structure but that use four different measures of length scale or characteristic pore size. If those pore size measures are different and one assumes that all of the models express the same fluid permeability, then one would expect that the scaling constants c_i would also be different. This section uses glass bead-pack and rock data to calculate the scaling constants that are associated with each model and to compare these experimentally determined values with theoretical and modeled values, when available. Table 1 shows a compilation of theoretically obtained, modeled, and experimental determinations of the scaling constants for each model. The theoretical sources are generally those of the model's creators. In addition, Bernabé (1995) has completed network modeling work that allows us to compare the scaling constants for the three models that existed when he published his work. It is clear from Table 1 that there is a wide range of values obtained by the various methods both within a certain model and between models.

We have attempted to compile experimental results to calculate the value of the scaling constant for each model. The scaling constant for each model has been calculated using equation 7 together with the measured permeability, porosity, formation factor, and length scale for each model; the last was calculated from equations 8, 11, 13, and 15 according to which model is being used.

Data sets in which the pore radius, measured permeability, porosity, and electrical properties, i.e., cementation exponent, formation factor, or connectedness, all are available are rare; however, we used 22 determinations made on glass bead packs from Chauveteau and Zaitoun (1981), Glover et al. (2006), and Glover and Walker (2009). It is important to note that the equations all depend on an effective grain radius. In the case of the bead packs, the effective grain radius was simply taken to be the same as the mean radius of the beads. Although we have no information regarding the distribution of bead ra-

Table 1. Scaling constants (previous work).

Model	Scaling constant (−)	Notes	Source
KC	$c_{KC} = 12$	2D	Theoretical Kostek et al. (1992)
	8	3D	Theoretical Kostek et al. (1992)
	28		Modeling Bernabé (1995)
SSJ	$c_{SSJ} = 8.00$	Tubes	Theoretical Johnson et al. (1986)
	12.00	Cracks	Theoretical Kostek et al. (1992)
	7.90	Cracks	Modeling Bernabé (1995)
	7.90	Tubes	Modeling Bernabé (1995)
	7.30	Mixed	Modeling Bernabé (1995)
	8.00	Tubes	Modeling Johnson and Schwartz (1989)
KT	$c_{KT} = 56.50$	Tubes	Theoretical Katz and Thompson (1986)
	32.55		Theoretical Banavar and Johnson (1987)
	21.18		Theoretical Le Doussal (1989)
	8.10		Modeling Bernabé (1995)
	8.10		Experimental Reed (1993)
	11.70		Experimental Reed (1993)
	15.50		Experimental Reed (1993)
RGPZ	$c_{RGPZ} = 8$	3D	Theoretical Glover and Walker (2009)

dii for the Chauveteau and Zaitoun data, we do have manufacturers' data and grain size distribution data from our own measurements in Glover et al. (2006) and Glover and Walker (2009). These take the form of laser diffraction measurements and optical microscopy image analysis. In all cases, the distribution of bead radii were monodisperse and extremely well constrained, with a standard deviation (SD) much less than the differences between bead sizes. It would be expected that a bidisperse or multidisperse bead pack with a range of bead sizes would provide different results from those obtained in this work. Such a study would be a useful further step to take.

The results are given in Figures 2 and 3. In Figure 2, the calculated scaling constants are shown as a function of the connectedness-permeability ratio. This ratio is a measure of the effectiveness of electrical transport to the effectiveness of hydraulic transport, which we arbitrarily designate by the letter W. Figure 3 shows the same scaling constant data but as a function of relevant length scale r_i, which is the reference microstructural gauge in each model. Table 2 contains the mean, maximum, minimum, and SDs of each set of scaling constant measurements for the glass bead packs for each model.

The calculated scaling constants for the glass bead packs remain constant with respect to the relevant scale length and the W number. The mean value is 17.973 ± 3.880, 2.467 ± 0.353, 2.796 ± 0.400, and 7.402 ± 1.058 for the KC, SSJ, KT, and RGPZ models, respectively. Here the uncertainties represent the SD of all of the measurements. Table 2 also shows the mean values broken down by source (Chauveteau and Zaitoun, 1981; Glover et al., 2006; Glover and Walker, 2009). Statistical tests on the mean scaling constants for each source and each model show that there is no statistical difference between the data from the three sources ($p<0.01$ for all pairs of cases); hence, the data from these three sources can be considered to come from a single source.

Figures 4 and 5 show the same analysis for 188 rock cores taken from a sand-shale sequence of the UK North Sea, provided by a major exploration and production company. The full data set was used by Glover and Walker (2009) and is analyzed fully therein. The cores are composed of consolidated sandstone with a small dispersed clay fraction that varies from 0% to 5% for individual samples and with a mean clay content of 1.5%. The data set is remarkably good for testing because it is fairly uniform, representing samples from a sand-shale sequence but also covering a wide range of effective grain sizes, porosities, and formation factors. The scaling length and scaling constants were calculated in exactly the same way as for the bead packs, differing only in that the basic length measurement is the grain size taken from image analysis measurements that are reported

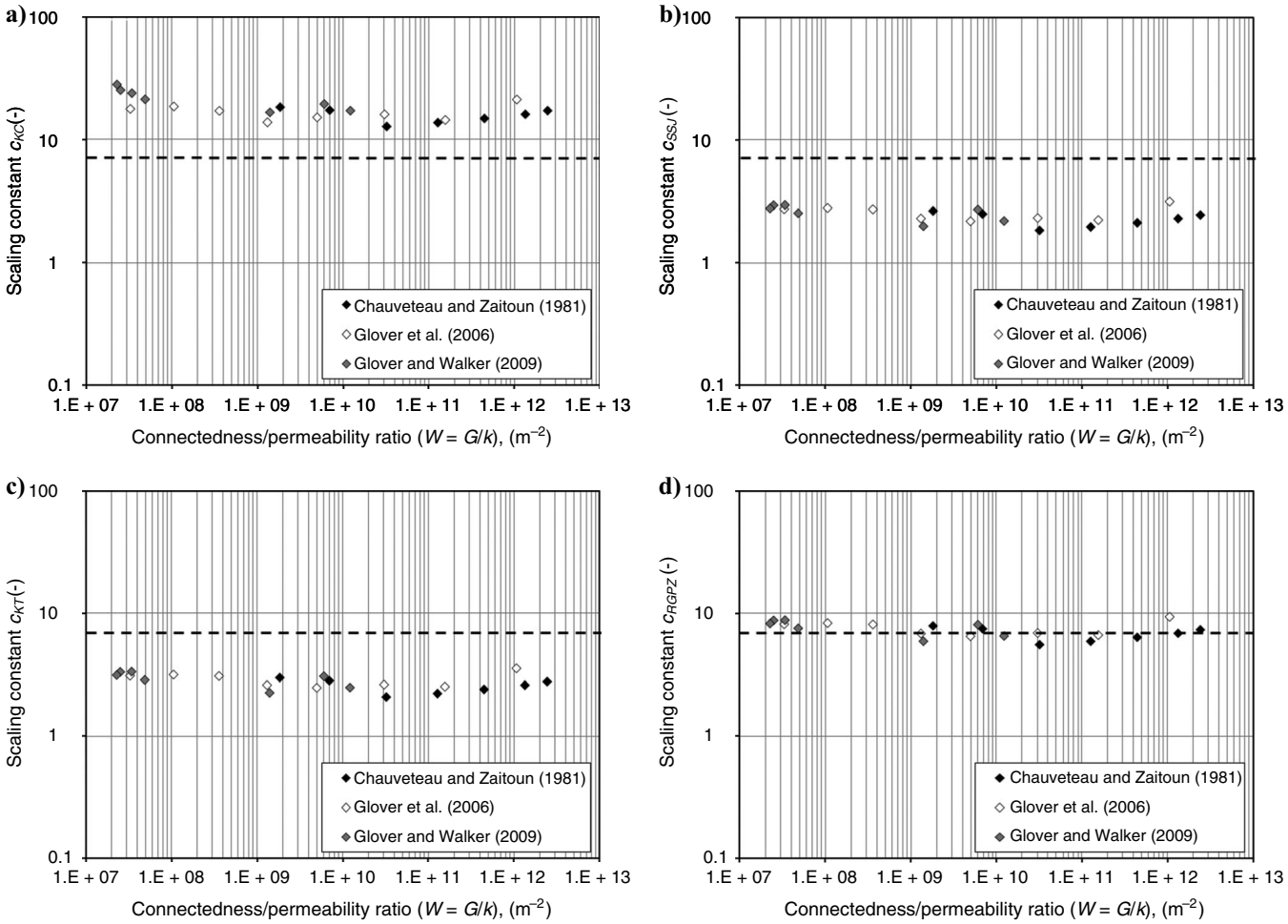

Figure 2. Scaling constants calculated from the permeability models of (a) KC, (b) SSJ, (c) KT, and (d) RGPZ, using data from 22 glass bead-pack experiments (Chauveteau and Zaitoun, 1981; Glover et al., 2006; Glover and Walker, 2009) as a function of the connectedness-permeability ratio W as defined in this work. The horizontal dashed line represents the value $c_i = 8$.

by Glover and Walker (2009). Although it is not explicitly stated in that paper, the mean grain size by image analysis took account only of the clastic fragments that made up the great majority of the rock samples (>98.5% on average); hence, the small fractions of clay material were not accounted for in the calculations. It would be an interesting study to repeat the calculations that were carried out in that work but with a sample set that contains significant clays and including them in the calculations.

In Figure 4, the calculated scaling constants are shown as a function of the connectedness-permeability ratio, whereas Figure 5 shows the scaling constants as a function of relevant length scale r_i. Table 2 also contains the mean, maximum, minimum, and SDs of each set of scaling constant measurements from the rock cores for each model.

Once again, it is clear that the scaling constant for the KT, SSJ, and RGPZ models remain constant with respect to the relevant scale length and the W number. The scaling constants for the SSJ and KT models are 3.14 ± 1.48 and 3.56 ± 1.68, respectively, whereas that for the RGPZ model is 9.43 ± 4.45. All are constant with both the relevant scale length and the W number; however, the KC model shows a systematic variation with respect to both the relevant scale length and the W number. We attribute this difference to the inability of the KC model to take account of the connectedness of the pores. The W and r_{KC} dependence did not occur for the glass bead packs for which the connectedness remains constant (at approximately 0.25) but is demonstrated in the rock data for which the connectedness varies between 0.0022 and 0.1100. The failure in the KC model has been noted before by Bernabé (1995), who remarked that the KC model did not perform well in his network modeling or in many other tests on natural materials (e.g., Scheidegger, 1974) because the KC model counts all pores regardless of whether they conduct. As also noted by Benson et al. (2006), the KC model is clearly too simple to describe the physics that occur in all but the simplest porous media. Mavko and Nur (1997) modified the KC model by including percolation terms. They show that the KC model with percolation allows a dramatically improved quantitative fit to permeability in clean, well-sorted rocks while preserving the simple third-power dependence on porosity over the entire range of porosities. This model retains the simplicity of the former KC model; however, a percolation porosity must be chosen empirically to give a good fit.

By contrast, the other three models all take account of the connectedness in three different ways: *Viz* local averaging with respect to the electrical field, the efficiency of fluid imbibition, and the use of parameters that describe electrical connectedness *via* electro-kinetic coupling, respectively. What is surprising is that all three provide reasonable and similar results.

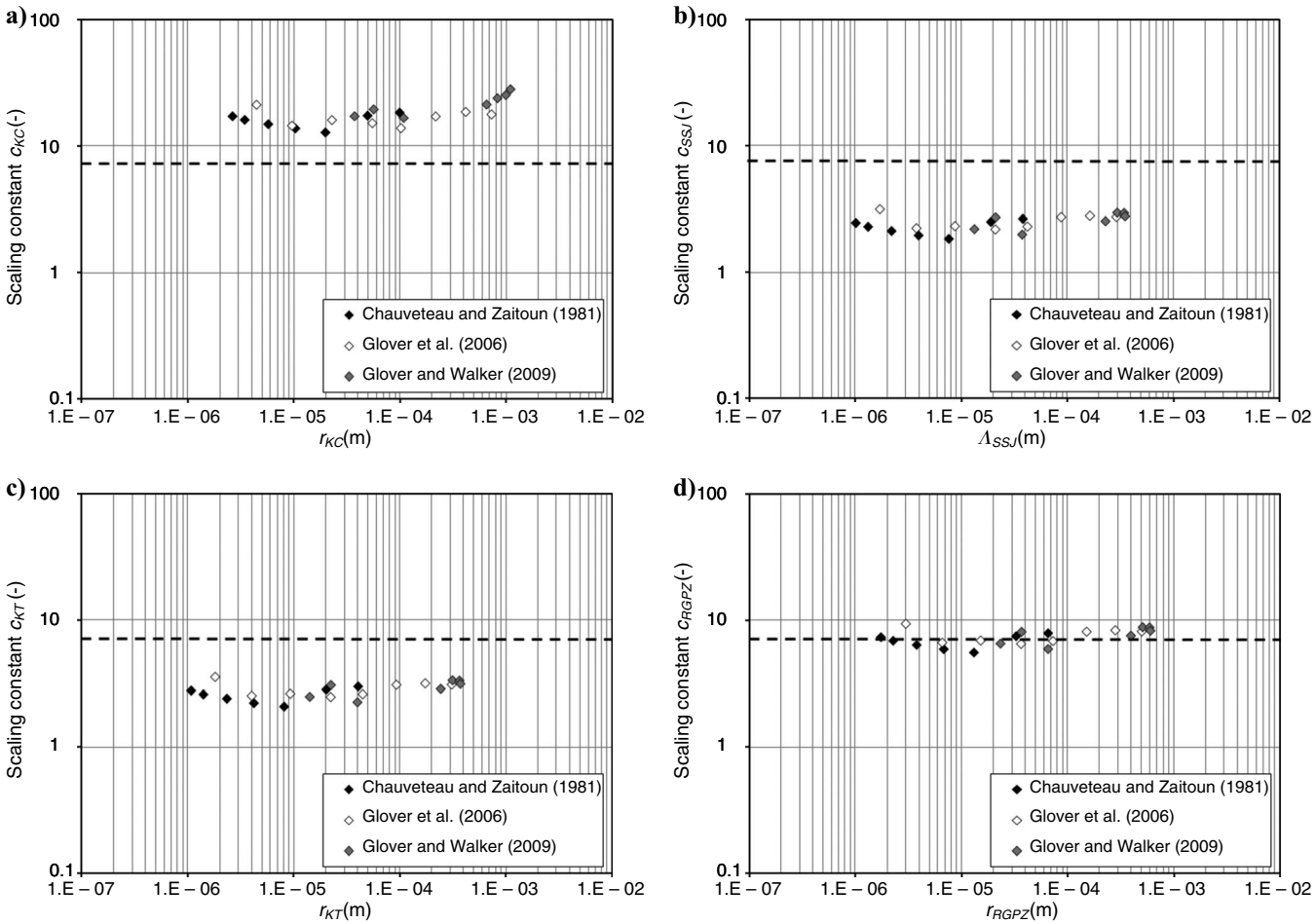

Figure 3. Scaling constants calculated from the permeability models of (a) KC, (b) SSJ, (c) KT, and (d) RGPZ, using data from 22 glass bead-pack experiments (Chauveteau and Zaitoun, 1981; Glover et al., 2006; Glover and Walker, 2009) as a function of the relevant length scale r_i for each model. The horizontal dashed line represents the value $c_i = 8$.

FREQUENCY-DEPENDENT ELECTROKINETICS

The coupling between fluid and electrical flow in porous media can be described in matrix form (De Groot & Mazur, 1962; Eccles et al., 2005):

$$\begin{bmatrix} Q \\ J \end{bmatrix} = - \begin{bmatrix} L_{11} & L_{12} \\ L_{21} & L_{22} \end{bmatrix} \begin{bmatrix} \nabla P \\ \nabla \varphi \end{bmatrix}, \tag{17}$$

where Q is the fluid flux (m/s), J is the current density (A/m^2), P is the fluid pressure (Pa), φ is the electric potential (V), and the matrix is composed of phenomenological coefficients L_{ij}.

The L_{22} term represents Ohm's law, whereas the L_{11} term represents Darcy's law. De Groot and Mazur (1962) used Onsager's relations to show that the terms that represent electrokinetic phenomena (L_{12} and L_{21}) are equal. These terms are a function of frequency and are referred to henceforth as $L(\omega)$.

According to equation 237 of Pride (1994), the frequency-dependent coefficient $L(\omega)$ can be expressed as

$$L(\omega) = L_o \left[1 - i \frac{m^*}{4} \frac{\omega}{\omega_t} \left(1 - 2 \frac{\tilde{d}}{\Lambda} \right)^2 \times \left(1 - i^{3/2} \tilde{d} \sqrt{\frac{\omega \rho_f}{\eta_f}} \right) \right]^{-1/2}, \tag{18}$$

where ω is the frequency (rad/s), ω_t is the electrokinetic transition frequency (rad/s), ρ_f is the density of the pore fluid (kg/m^3), η_f is the dynamic viscosity of the pore fluid (Pa.s), and $\tilde{d}$ is the characteristic length associated with the width of the double layer. The dimensionless number m^* was defined by Pride (1994) in terms of the electrical tortuosity τ_e (Note that Pride named this parameter m; we use the form m^* to avoid confusion with the cementation exponent.)

$$m^* \equiv \frac{\phi \Lambda^2}{\tau_e k} = \frac{\phi \chi_e \Lambda^2}{k} = \frac{G \Lambda^2}{k}, \tag{19}$$

where ϕ is the porosity of the porous medium, and k is the permeability of the sample (m^2). We also display it in terms of the electrical connectivity of the pore network χ_e ($\chi_e = 1/\tau_e$) and the connectedness of the pore network G ($G = \phi \chi_e$) after Glover (2009). The symbol Λ (which is identical with Λ_{SSJ} used previously in this paper) is the characteristic length scale associated with the pore size as defined in a series of papers by Johnson et al. (1986), Johnson and Sen (1988), Schwartz et al. (1989), and Johnson and Schwartz (1989).

By applying equations 4 and 7 of Glover and Walker (2009), it can be proved that the dimensionless number m^* is the same as the pore space variable that was introduced by Bernabé (1995) as c_3 and used thereafter by Glover et al. (2006) as a:

$$m^* \equiv \frac{\phi \Lambda^2}{\tau_e k} = \frac{\phi \chi_e \Lambda^2}{k} = \frac{8 \Lambda^2}{r_{eff}^2} = a. \tag{20}$$

Here r_{eff} is identical to r_{RGPZ}, the measure of characteristic pore radi-

Table 2. Scaling constants (experimental values).

	Scaling constant (−)				
	Glass beads ($n = 22$)				Rock cores ($n = 188$)
Data subset	All data	Chauveteau and Zaitoun (1981)	Glover et al. (2006)	Glover and Walker (2009)	All data
KC					
Mean	17.973	15.757	16.750	21.587	477.47
SD	3.857	2.018	2.420	4.268	1046.00
Minimum	12.817	12.817	13.805	16.542	12.14
Maximum	27.981	18.310	21.145	27.981	9767.00
SSJ					
Mean	2.467	2.258	2.553	2.579	3.14
SD	0.353	0.292	0.343	0.370	1.48
Minimum	1.846	1.846	2.183	1.983	0.29
Maximum	3.141	2.637	3.141	2.947	11.91
KT					
Mean	2.796	2.559	2.893	2.923	6.56
SD	0.400	0.331	0.389	0.419	1.68
Minimum	2.092	2.092	2.475	2.247	0.33
Maximum	3.559	2.988	3.559	3.340	13.49
RGPZ					
Mean	7.402	6.773	7.659	7.737	9.43
SD	1.058	0.876	1.030	1.110	4.45
Minimum	5.537	5.537	6.550	5.949	0.87
Maximum	9.422	7.910	9.422	8.841	35.72

us that is based on electrokinetic considerations that were defined by Glover and Walker (2009).

From equation 20, it is possible to write

$$k = \frac{G}{a}\Lambda^2. \tag{21}$$

Remembering that this equation is derived from the combination of the work of Pride (1994) and Glover and Walker (2009), equation 21 indicates that the permeability is directly proportional to the connectedness of the pore network G and the square of the dynamic hydraulic radius of the SSJ model and inversely proportional to the a factor. In other words, the equations developed by Pride (1994), Glover et al. (2006), and Glover and Walker (2009) are consistent with the SSJ model of Johnson et al. (1986), Johnson and Sen (1988), Schwartz et al. (1989), Johnson and Schwartz (1989), and Kostek et al. (1992), as well as with the findings of Bernabé (1995) in his modeling study, with $a = m^* = c_3 = c_{SSJ} = c_{KT} = c_{RGPZ}/3$. This is consistent with the experimental results from glass bead packs and rock cores described previously in this paper (Table 2). The glass bead pack data give $c_{SSJ} = 2.467 \pm 0.353$ and $c_{KT} = 2.796 \pm 0.400$, which compare favorably with $8/3 = 2.666$, and $c_{RGPZ} = 7.402 \pm 1.058$, which is close to 8. The rock core data give $c_{SSJ} = 3.14 \pm 1.48$ and $c_{KT} = 3.56 \pm 1.68$, which are comfortably within 1 SD of the value $8/3 = 2.666$, and $c_{RGPZ} = 9.43 \pm 4.45$, which is also comfortably within 1 SD of 8. We may say, therefore, that for the data sets that we have used, $a = m^* = c_3 = c_{SSJ} \approx c_{KT} \approx 8/3$ and $c_{RGPZ} \approx 8$.

TRANSITION FREQUENCY AND PORE SCALE LENGTH

Because the frequency-dependent streaming potential is caused by frequency-dependent fluid flow, it might be expected that the two phenomena would have identical frequency behaviors. The physical cause of the transition frequency in both frequency-dependent flow and frequency-dependent streaming potential is to be found in the transition in the flow regime from viscous to inertial flow. As the frequency increases, inertial effects start to retard the motion of the fluid within the pore space (Reppert et al., 2001). At the high frequencies, the flow becomes inefficient and requires more energy to displace the same amount of liquid the same distance; hence, at frequencies higher than the transition from viscous to inertial flow, more pressure is required to shear the same quantity of ions in the diffuse layer than at low frequencies when viscous flow dominates, thereby causing lower streaming potentials at high frequencies.

The flow regime is determined locally by the local fluid velocity and the local pore structure. Individual pores undergo the transition from viscous to inertial flow at different frequencies because they

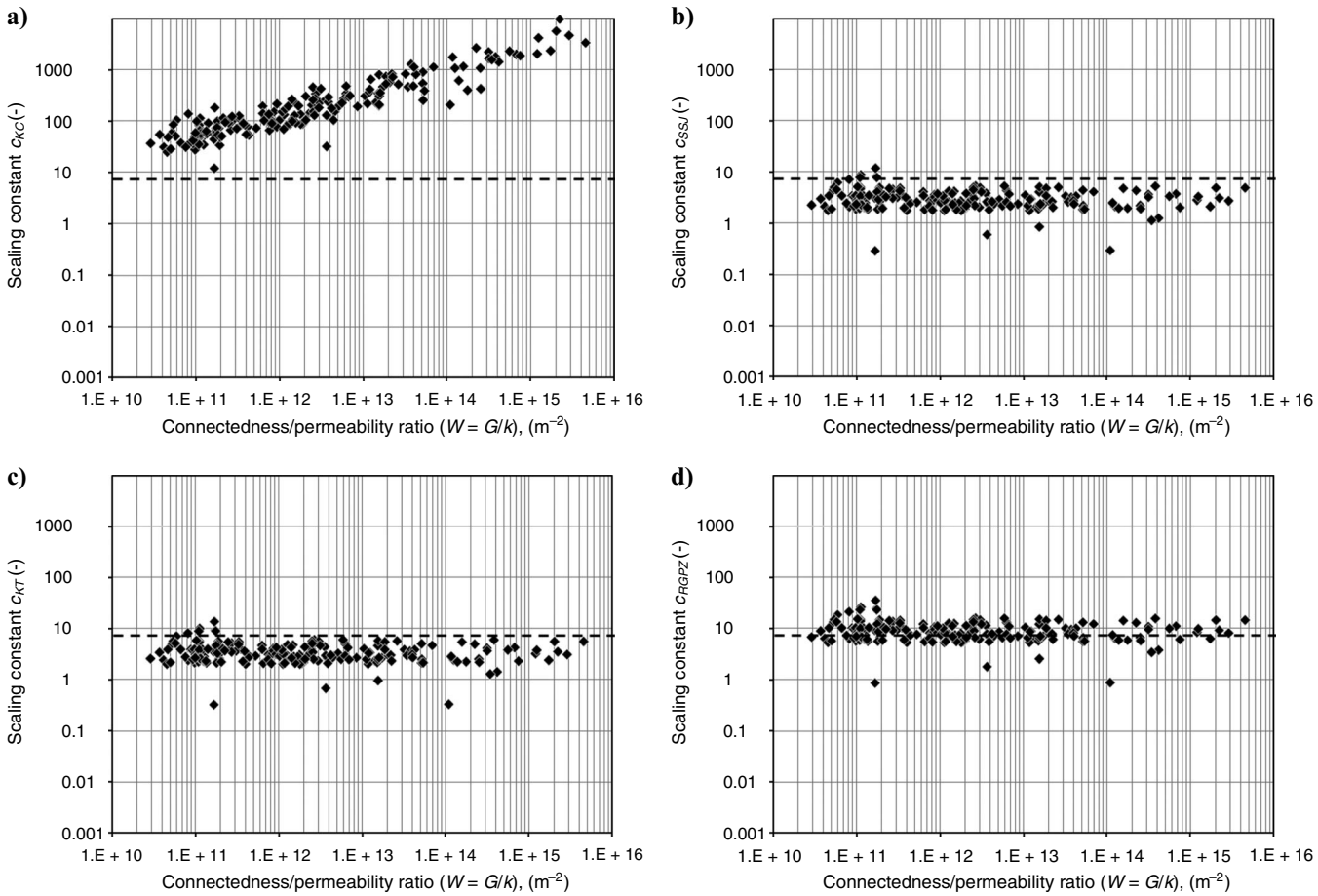

Figure 4. Scaling constants calculated from the permeability models of (a) KC, (b) SSJ, (c) KT, and (d) RGPZ, using data from 188 rock cores from a sand-shale sequence of the U.K. North Sea (Glover and Walker, 2009) as a function of the connectedness-permeability ratio W as defined in this work. The horizontal dashed line represents the value $c_i = 8$.

conduct fluid at different rates and are connected differently to the global flow network. The measured transition frequency is the result of a set of transition frequencies that arise from all of the different pores in the rock. This is an idea that not only underpins the formulation of the SSJ model but also is linked to percolation problems in porous media. Because the KT model uses a capillary radius at breakthrough during an invasion percolation process, we can attribute the apparent accordance between the SSJ and KT models to the transition from viscous to inertial flow. The mechanism of transition from viscous to inertial flow on a local pore scale also provides a physical reason for why the transition frequency should be related to the characteristic pore radius of the rock.

It is not, in fact, strictly true that the streaming potential has the same frequency behavior as fluid flow. At frequencies greater than the transition frequency, there is a difference in the behavior that is caused by the dominance of a second-order effect in the high-frequency hydraulic flow solution close to the pore walls where the diffuse layer exists and thus has a disproportionate effect on the high-frequency behavior of the streaming potential (Reppert et al., 2001).

The zero-frequency electrokinetic coefficient L_o in equation 18 is given by Pride (1994) as

$$L_o = -\frac{\varepsilon_o \varepsilon_f \zeta}{\eta_f}\frac{1}{F}\left(1 - 2\frac{\widetilde{d}}{\Lambda}\right) \tag{22}$$

where ε_o is the permittivity of a vacuum ($\approx 8.854 \times 10^{-12}$ F/m), ε_f is the electric permittivity of the pore fluid (≈ 80), and ζ is the zeta potential (V). According to Pride (1994), the term $(1 - 2\widetilde{d}/\Lambda)$ is a correction term that amounts, at most, to a few percent. It depends on $\widetilde{d}$, which is the characteristic length associated with the width of the double layer, and Λ, which is a characteristic length scale associated with the pore size. Because $\widetilde{d} \ll \Lambda$ for most geological regimes, the correction term is small under the thin double-layer assumption.

Assuming formally that $\widetilde{d} \ll \Lambda$, we can rewrite equations 18 and 22 as

$$\begin{aligned} L(\omega) &= L_o\left[1 - i\frac{\phi \chi_e \Lambda^2}{4k}\frac{\omega}{\omega_t}\right]^{-1/2} \\ &= L_o\left[1 - i\frac{m^*}{4}\frac{\omega}{\omega_t}\right]^{-1/2} \quad \text{with} \quad L_o = -\frac{\varepsilon_o \varepsilon_f \zeta}{\eta_f}\frac{1}{F} \end{aligned} \tag{23}$$

and using equations 4 and 7 of Glover and Walker (2009) as

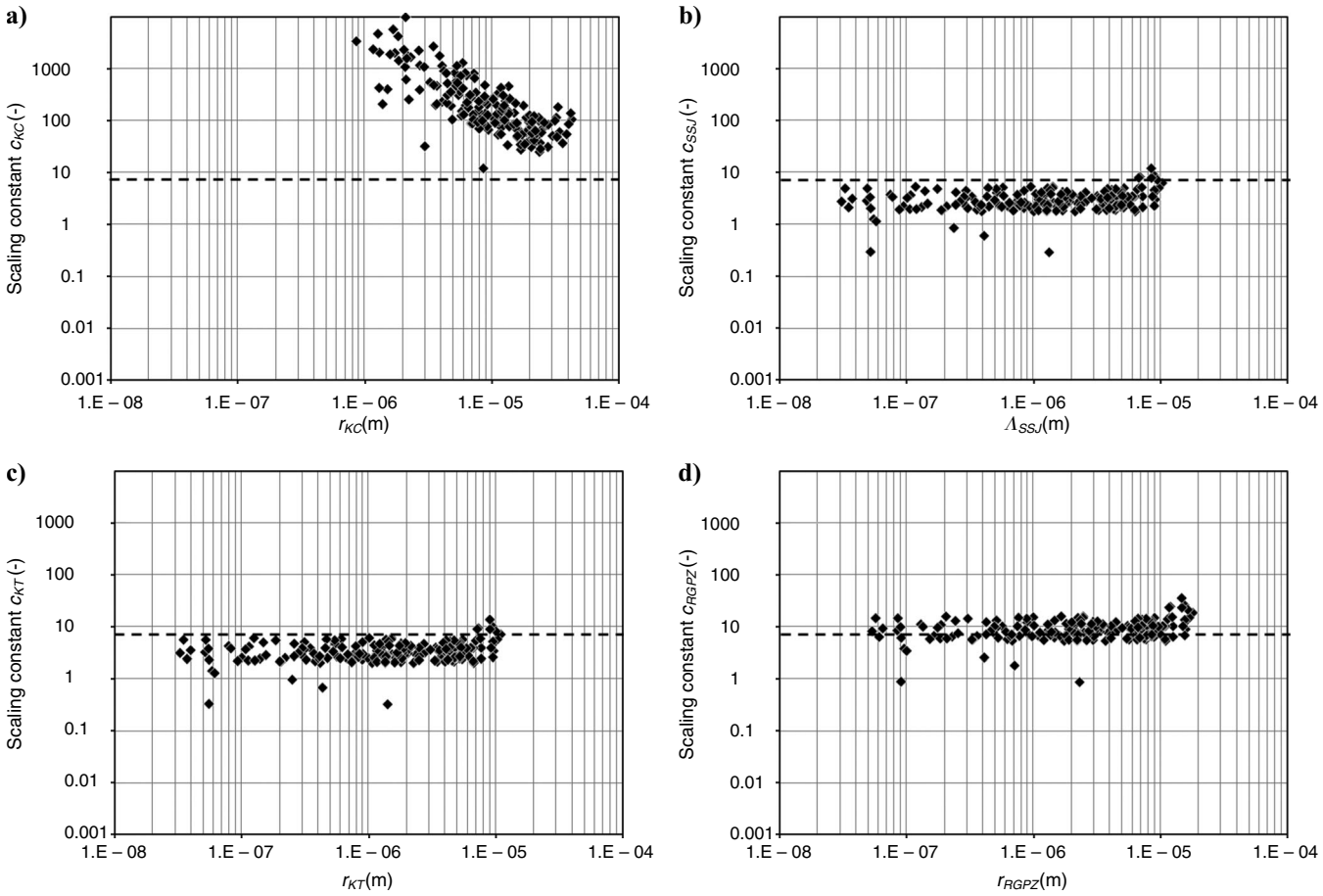

Figure 5. Scaling constants calculated from the permeability models of (a) KC, (b) SSJ, (c) KT, and (d) RGPZ, using data from 188 rock cores from a sand-shale sequence of the U.K. North Sea (Glover and Walker, 2009) as a function of the relevant length scale r_i for each model. The horizontal dashed line represents the value $c_i = 8$.

$$L(\omega) = L_o\left[1 - 2i\left(\frac{\Lambda}{r_{eff}}\right)^2\frac{\omega}{\omega_t}\right]^{-1/2} = L_o\left[1 - i\frac{a}{4}\frac{\omega}{\omega_t}\right]^{-1/2}. \quad (24)$$

Comparison of equations 23 and 24 shows once again that $m^* = a$.

If we take $a = 8/3$, as has been demonstrated experimentally previously in this work, equation 24 becomes

$$L(\omega) = L_o\left[1 - i\frac{2}{3}\frac{\omega}{\omega_t}\right]^{-1/2} \quad (25)$$

The transition frequency ω_t has been defined by Pride (1994) as

$$\omega_t \equiv \frac{\phi}{\tau_e k}\frac{\eta_f}{\rho_f}, \quad (26)$$

and can be rewritten using equation 7 of Glover and Walker (2009) to give

$$\omega_t = \frac{\phi\chi_e}{k}\frac{\eta_f}{\rho_f} = \frac{8}{r_{eff}^2}\frac{\eta_f}{\rho_f}, \quad (27)$$

which is consistent with the result for capillary tubes found by Reppert et al. (2001) in their equation 33.

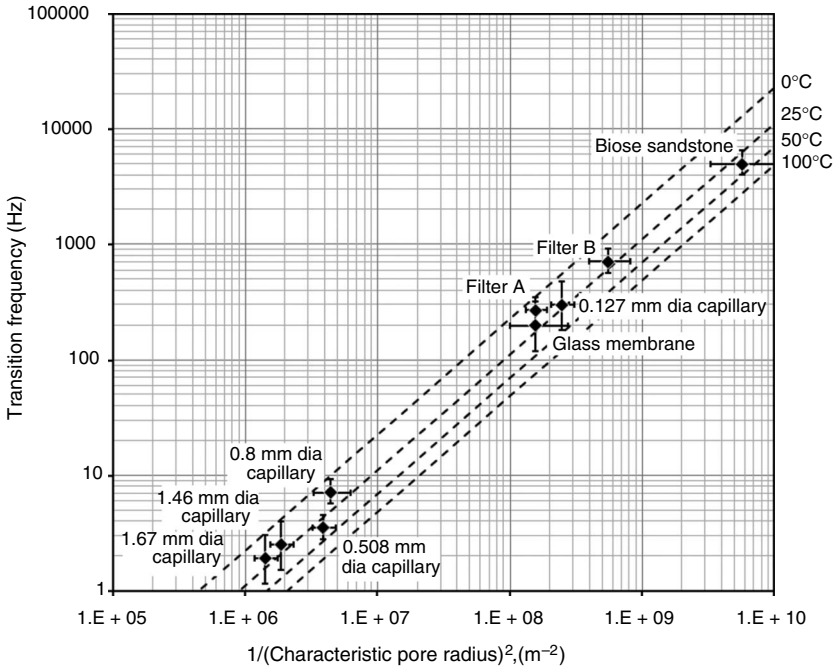

Figure 6. The electrokinetic transition frequency as a function of the inverse square characteristic pore size. The dashed lines represent the result of equation 27 at four different temperatures for water as the pore fluid and with the respective densities and viscosities: For T = 0°C, $\eta_f = 1.79\times10^{-3}$ Pa.s and $\rho_f = 10^3$ kg/m^3; for T = 25°C, $\eta_f = 0.89\times10^{-3}$ Pa.s and $\rho_f = 997$ kg/m^3; for T = 50°C, $\eta_f = 0.547\times10^{-3}$ Pa.s and $\rho_f = 988$ kg/m^3; for T = 1000°C, $\eta_f = 0.282\times10^{-3}$ Pa.s and $\rho_f = 589.67$ kg/m^3 (Lide, 2009). Measured data from filter A and filter B come from Reppert (2000) and Reppert et al. (2001); the nominally 0.8 mm and 0.127 mm diameter glass capillary tube and the Boise sandstone data are from Reppert (2000); the 1.67 mm and 1.46 mm diameter glass capillary data are from Packard (1953); the 0.508 mm diameter glass capillary data are from Sears and Groves (1977); and the Corning fritted glass membrane data are from Cooke (1955). Uncertainties are from various sources described in the text.

Equation 27 predicts that the transition frequency depends on the inverse characteristic pore radius squared. It is difficult to test this hypothesis because of the lack of AC electrokinetic data. Figure 6 shows a plot of transition frequency as a function of inverse characteristic pore radius squared for what we believe to be all of the existing data. The figure contains transition frequency data for two ceramic filters, five capillary tubes, one sample of Boise sandstone, and one Dow Corning fritted glass membrane. The ceramic filter data were from Reppert (2000) and Reppert et al. (2001): Filter A had a manufacturer mean pore radius quoted in the range of 72.50 to 87.00 μm, from which we derived a mean value of 79.75 μm and used the range to define the error bars on the figure. The authors quote a transition frequency of 269 Hz for filter A. Similarly, filter B had a mean pore radius quoted in the range of 35.0 to 50.0 μm, from which we derived a mean value of 42.5 μm and the respective uncertainty estimation and a measured transition frequency of 710 Hz. The capillary tube data were from Packard (1953), Sears and Groves (1978), Reppert (2000), and Reppert et al. (2001). We assigned a mean capillary radius according to the data presented by these authors and used their values for the uncertainty in the measurement when available, taking care to account for conversion to capillary radius and conversion from obsolete units. When an author-defined error was not available, we assigned an error of 10%, which we consider to be conservative. The sole rock data available are those for a sample of Boise sandstone from Reppert (2000). The author gives a transition frequency of 5000 Hz but no independent measurement for the mean pore size of the Boise sandstone; however, we obtained a value of 13.22 ± 4.09 μm by using the method of Glover et al. (2006) to invert the author's measured permeability data and then checking for consistency with a detailed microstructural study of Boise sandstone by Schlueter et al. (1997). The fritted glass membrane data were from Cooke (1955). Again, the author gives no pore size information; however, his description of the samples was sufficiently detailed for the employees of the Dow Corning Glass Museum to find a mean pore radius and range in their archives (80 ± 20 μm).

In Figure 6, the straight lines are not fitted to the data but are the results of equation 27 for water viscosities and densities at 0°C, 25°C, 50°C, and 100°C, taken from Lide (2009). (For a temperature of 25°C, the viscosity is $\eta_f = 0.89\times10^{-3}$ Pa.s, and the density is $\rho_f = 0.997\times10^3$ kg/m^3.) It is clear that the equation works very well with the supposition that all of the data were measured at approximately 25°C and bearing in mind the lack of available data, the age of some of the data, and the possibility that the salinity of the pore fluids was different from those that were used to generate the theoretical curves used here. In corollary, the success of equation 27 in fitting the available transition frequency data is an indirect confirmation that the previous theoretical development in this paper and that of the previous authors is valid. Furthermore, the transition frequency seems to depend on only one matrix pa-

rameter: The effective pore size. Thankfully, there seems to be no dependence on mineral type, zeta potential, pH, *etc*, that usually make the detailed analysis of the electrical properties of rocks too complex.

Finally, equation 27 may also be expressed in terms of the W number defined previously in this work, which is the ratio of the connectedness of the porous medium to its permeability:

$$\omega_t = \frac{G}{k}\frac{\eta_f}{\rho_f} = W\frac{\eta_f}{\rho_f}; \tag{28}$$

hence, the permeability may be predicted by using

$$k = \frac{G}{\omega_t}\frac{\eta_f}{\rho_f} = \frac{\eta_f}{\rho_f \omega_t F}. \tag{29}$$

Although this equation may not be useful for predicting permeability at the present time, we are investigating whether there exists a high-quality proxy for the transition frequency that is measurable downhole.

CONCLUSIONS

Four important models that describe the fluid permeability on porous media have been compared and been found to follow the same generic form even though they are derived from very different physics. The difference between the models depends on which scale length they use and which scaling constant is then used to validate the model. We have studied the scale lengths and scaling constants both theoretically and using experimental data.

The KC model did not perform well, as has been noted before by many authors (e.g., Scheidegger, 1974; Bernabé, 1995), and should no longer be used. The problem with this model is that it takes no account of the connectedness of the pore network. The SSJ, the KT, and the RGPZ models all performed well when used with their respective length scales and scaling constants. It was noted that the SSJ and KT models were extremely similar, such that $c_{SSJ} \approx c_{KT}$ and $\Lambda_{SSJ} \approx r_{KT}$ despite the disparity in their physical derivation. Comparison of the models with experimental data from 22 bead packs and 188 rock cores from a sand-shale sequence in the U.K. sector of the North Sea has provided values for the scaling constants for each model, with $a = m^* = c_3 = c_{SSJ} \approx c_{KT} \approx 8/3$ and $c_{RGPZ} \approx 8$. Use of time-dependent electrokinetic theory allows us also to equate some of the scaling constants to the m value used by Pride (1994), the a value used by Glover et al. (2006), and the c_3 value used by Bernabé (1995): $a = m^* = c_3 = c_{SSJ} \approx c_{KT}$ and $a = m^* = c_3 = c_{RGPZ}/3$.

Furthermore, we have derived a relationship between the electrokinetic transition frequency and the RGPZ scale length and validated it using experimental data from ceramic filters, glass membranes, capillary tubes, and one sandstone. Because we believe that these are the only time-dependent electrokinetic data available in the scientific literature, we state strongly that there is a real need for more AC electrokinetic experiments to be carried out, especially on geological porous media.

It is clear from this work and that of others that the KC model is not sufficiently reliable for its continued use. The SSJ model works well but is impractical because the local electrical field cannot be macroscopically measured; hence, the practical implication of this work for permeability prediction is that the KT model should be used when fluid imbibition data are available, whereas the RGPZ model should be used when electrical data are available. If neither is available but core plugs are, then we recommend that the permeability be measured on them. Alternatively, permeabilities may be derived from downhole nuclear magnetic resonance measurements directly or by combining them with electrical measurements (Glover et al., 2006).

ACKNOWLEDGMENTS

This work has been made possible by funding from the Natural Sciences and Engineering Research Council of Canada (NSERC) Discovery Grant Programme. We thank the associate editor, José Carcione; the reviewer, Phil Benson; and another, anonymous reviewer for their constructive comments and additions.

REFERENCES

Banavar, J. R., and D. L. Johnson, 1987, Characteristic pore sizes and transport in porous media: Physical Review B: Condensed Matter and Materials Physics, **35**, no. 13, 7283–7286, doi: 10.1103/PhysRevB.35.7283.

Benson, P. M., P. G. Meredith, and A. Schubnel, 2006, Role of void space geometry in permeability evolution in crustal rocks at elevated pressure: Journal of Geophysical Research, **111**, B12, B12203, doi: 10.1029/2006JB004309.

Bernabé, Y., 1995, The transport properties of networks of cracks and pores: Journal of Geophysical Research, **100**, B3, 4231–4241, doi: 10.1029/94JB02986.

Chauveteau, G., and A. Zaitoun, 1981, Basic rheological behavior of xanthan polysaccharide solutions in porous media: Effect of pore size and polymer concentration, *in* F. J. Fayers, ed., Enhanced oil recovery, Elsevier, 197–212.

Cooke, C. E., 1955, Study of electrokinetic effects using sinusoidal pressure and voltage: The Journal of Chemical Physics, **23**, no. 12, 2299–2303, doi: 10.1063/1.1740742.

De Groot, S. R., and P. Mazur, 1962, Non-equilibrium thermodynamics: North-Holland.

Eccles, D., P. R. Sammonds, and O. C. Clint, 2005, Laboratory studies of electrical potential during rock failure: International Journal of Rock Mechanics and Mining Sciences, **42**, no. 7–8, 933–949, doi: 10.1016/j.ijrmms.2005.05.018.

Glover, P. W. J., 2009, What is the cementation exponent? A new interpretation: The Leading Edge, **28**, 82–85, doi: 10.1190/1.3064150.

Glover, P. W. J., and N. Déry, 2010, Streaming potential coupling coefficient of quartz glass bead packs: Dependence on grain diameter, pore size, and pore throat radius: Geophysics, **75**, this issue.

Glover, P. W. J., and E. Walker, 2009, A grain size to effective pore size transformation derived from an electro-kinetic theory: Geophysics, **74**, no. 1, E17–E29, doi: 10.1190/1.3033217.

Glover, P. W. J., I. I. Zadjali, and K. A. Frew, 2006, Permeability prediction from MICP and NMR data using an electrokinetic approach: Geophysics, **71**, no. 4, F49–F60, doi: 10.1190/1.2216930.

Johnson, D. L., and L. M. Schwartz, 1989, Unified theory of geometrical effects in transport properties of porous media: Presented at 30th Annual Symposium, Society of Petrophysicists and Well Log Analysts paper E, 1–25.

Johnson, D. L., and P. N. Sen, 1988, Dependence of the conductivity of a porous medium on electrolyte conductivity: Physical Review B: Condensed Matter and Materials Physics, **37**, no. 7, 3502–3510, doi: 10.1103/PhysRevB.37.3502.

Johnson, D. L., J. Koplik, and L. M. Schwartz, 1986, New pore-size parameter characterizing transport in porous media: Physical Review Letters, **57**, no. 20, 2564–2567, doi: 10.1103/PhysRevLett.57.2564.

Katz, A. J., and A. H. Thompson, 1986, Quantitative prediction of permeability in porous rock: Physical Review B: Condensed Matter and Materials Physics, **34**, no. 11, 8179–8181, doi: 10.1103/PhysRevB.34.8179.

Katz, A. J., and A. H. Thompson, 1987, Prediction of rock electrical conductivity from mercury injection measurements: Journal of Geophysical Research, **92**, B1, 599–607, doi: 10.1029/JB092iB01p00599.

Kostek, S., L. M. Schwartz, and D. L. Johnson, 1992, Fluid permeability in porous media: Comparison of electrical estimates with hydrodynamical calculations: Physical Review B: Condensed Matter and Materials Physics, **45**, no. 1, 186–195, doi: 10.1103/PhysRevB.45.186.

Le Doussal, P., 1989, Permeability versus conductivity for porous media with wide distribution of pore sizes: Physical Review B: Condensed Matter and Materials Physics, **39**, no. 7, 4816–4819, doi: 10.1103/PhysRevB.39.4816.

Lide, D. R., 2009, Handbook of chemistry and physics: 90th ed.: CRC Press.

Mavko, G., and A. Nur, 1997, The effect of a percolation threshold in the Kozeny-Carman relation: Geophysics, **62**, 1480–1482, doi: 10.1190/1.1444251.
Packard, R. G., 1953, Streaming potentials across glass capillaries for sinusoidal pressure: The Journal of Chemical Physics, **21**, no. 2, 303–307, doi: 10.1063/1.1698876.
Pride, S., 1994, Governing equations for the coupled electro-magnetics and acoustics of porous media: Physical Review B: Condensed Matter and Materials Physics, **50**, no. 21, 15678–15696, doi: 10.1103/PhysRevB.50.15678.
Reed, J. S., 1993, Liquid permeability of packed particles: Why perpetuate the Carmen-Kozeny model?: Journal of the American Ceramic Society, **76**, no. 2, 547–548, doi: 10.1111/j.1151-2916.1993.tb03824.x.
Reppert, P. M., 2000, Electrokinetics in the Earth: Ph.D. thesis, Massachusetts Institute of Technology.
Reppert, P. M., F. D. Morgan, D. P. Lesmes, and L. Jouniaux, 2001, Frequency-dependent streaming potential: Journal of Colloid and Interface Science, **234**, no. 1, 194–203, doi: 10.1006/jcis.2000.7294.
Revil, A., and L. M. Cathles III, 1999, Permeability of shaly sands: Water Resources Research, **35**, no. 3, 651–662, doi: 10.1029/98WR02700.
Scheidegger, A. E., 1974, The physics of flow through porous media: University of Toronto Press.
Schlueter, E. M., R. W. Zimmerman, P. A. Witherspoon, and N. G. W. Cook, 1997, The fractal dimension of pores in sedimentary rocks and its influence on permeability: Engineering Geology, **48**, no. 3–4, 199–215, doi: 10.1016/S0013-7952(97)00043-4.
Schwartz, L. M., P. N. Sen, and D. L. Johnson, 1989, Influence of rough surfaces on electrolytic conduction in porous media: Physical Review B: Condensed Matter and Materials Physics, **40**, no. 4, 2450–2458, doi: 10.1103/PhysRevB.40.2450.
Sears, A. R., and J. N. Groves, 1978, The use of oscillating laminar flow streaming potential measurements to determine the zeta potential of a capillary surface: Journal of Colloid and Interface Science, **65**, no. 3, 479–482, doi: 10.1016/0021-9797(78)90099-1.